Journal of Catalysis **202,** 324–339 (2001)
doi:10.1006/jcat.2001.3292, available online at http://www.idealibrary.com on IDEAL®

Alkene Protonation Enthalpy Determination from Fundamental Kinetic Modeling of Alkane Hydroconversion on Pt/H–(US)Y-Zeolite

J. W. Thybaut,* G. B. Marin,*,[1] G. V. Baron,† P. A. Jacobs,‡ and J. A. Martens‡

*Laboratorium voor Petrochemische Techniek, Universiteit Gent, Krijgslaan 281, B-9000 Gent, Belgium; †Chemie Ingenieurstechniek, Vrije Universiteit Brussel, Pleinlaan 2, B-1050 Brussel, Belgium; and ‡Centrum voor Oppervlaktechemie en Katalyse, Katholieke Universiteit Leuven, Kasteelpark Arenberg 23, B-3001 Heverlee, Belgium

Received February 26, 2001; revised May 16, 2001; accepted May 21, 2001

Alkane, c.q., C_5 to C_{12}, hydrocracking was performed on Pt/H–Y-zeolite and on Pt/H–USY-zeolites with Si/Al ratio of 13 and 30 at temperatures of 506–563 K, pressures of 0.45–1.5 MPa, and molar hydrogen to hydrocarbon ratio's in the 4.23–250 range. The catalytic conversion was described with a fundamental molecular model, relying on experimentally determined physisorption equilibria and on a network of elementary reactions according to the bifunctional reaction scheme. The three zeolite samples showed substantial differences in activity, but not in selectivity. The activity differences among the zeolites mainly resulted from differences in both the number of acid sites and the average acid strength, while differences in physisorption effects for these zeolite samples were of minor importance. On each catalyst, the reactivity of alkanes increased with carbon number. This tendency was related to three phenomena: (1) physisorption of heavier molecules was more favorable; (2) the reaction network and the number of parallel reactions became larger with larger molecules, and (3) in the range of carbon numbers from C_5 to C_8, the stabilization of alkylcarbenium ions and, hence, their concentration increased with increasing size and electron donating property of alkyl-substituents. The differences in average acid strength between the three catalysts were quantified with alkene protonation enthalpy values extracted from the model. The kinetic parameters obtained for a reference hydrocarbon component and a reference Pt/H–(US)Y-type zeolite are adaptable to any other hydrocarbon and any other Pt/H–(US)Y-type catalyst by adjusting the standard protonation enthalpy.

Key Words: **hydrocracking; alkanes; alkenes; carbon number; Y- and USY-zeolite; acid strength; kinetic modeling; protonation enthalpy.**

1. INTRODUCTION

Hydrocracking and hydroisomerization are important refinery processes for upgrading heavy oil fractions such as vacuum gasoil into more valuable lighter fractions such as diesel, aviation fuel, and lubricating oil (1, 2). Laboratory studies of such processes are commonly performed with model hydrocarbon components, based on the assumption that these are representative of the components of a typical industrial feed.

The reaction scheme of a model alkane is depicted in Fig. 1. Hydrocracking occurs via a bifunctional reaction scheme (3, 4). The alkane is physisorbed in the zeolite pores (5), subsequently, it is chemisorbed on a metal such as Pt and dehydrogenated into an alkene. This alkene intermediate desorbs from the metal and migrates to an acid site of the catalyst, where it is protonated and yields an alkylcarbenium ion. The alkylcarbenium ion can undergo isomerization reactions such as hydride-shifts (HS), alkyl-shifts (AS), and branching via protonated cyclopropanes (PCP), which yields a different alkylcarbenium ion. It may also be susceptible to cracking reactions, i.e., β-scissions, which give rise to the formation of a smaller alkylcarbenium ion and an alkene fragment. The resulting alkylcarbenium ion undergoes deprotonation and becomes a physisorbed alkene thus regenerating the acid site. Hydrogenation on the metal function results in the formation of the reaction product. Experimental reaction conditions can be chosen so that the acid-catalyzed reaction steps are rate determining while the metal-catalyzed hydrogenation and dehydrogenation reactions are in quasi-equilibrium, i.e., conditions of so-called "ideal" hydrocracking (6).

Hydroxyl groups bridging a silicon atom and an aluminum atom in the tetrahedral oxide framework are generally accepted as the active sites in Brönsted acid-catalyzed conversions on zeolites. Quantumchemical calculation of the interaction of a light alkene with an acid site of a zeolite framework fragment predicts the formation of surface alkoxide species (7–9). For branched hydrocarbons giving rise to tertiary alkylcarbenium ions, surface alkoxide formation is for sterical reasons rather unlikely (10). The kinetic model used in this work was based on alkylcarbenium ions as reaction intermediates, although the same rate equations also hold for alkoxide-type intermediates. This follows from the derivation of the rate equations (11, 12).

The acidity of H–Y-type zeolite can be modified by framework dealumination (13, 14). The catalytic activity on

[1] To whom correspondence should be addressed. E-mail: Guy.Marin@rug.ac.be.

0021-9517/01 $35.00

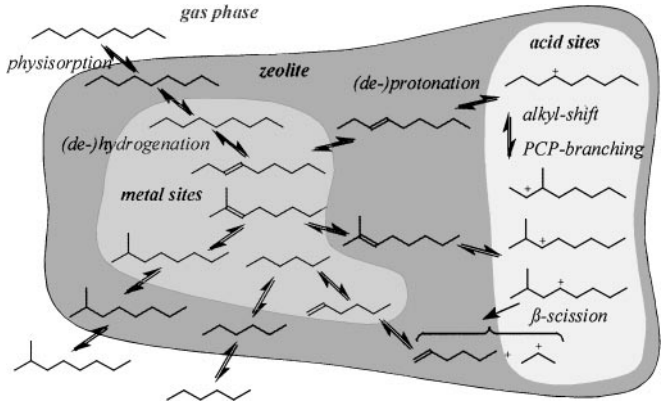

FIG. 1. Hydrocracking reaction scheme.

catalyst weight basis plotted versus framework aluminum content typically shows a "volcano" curve, with maximum activity at a framework composition that is specific for the feedstock (15–21). The "volcano" shape has been often explained based on aluminum concentration changes of the tetrahedral oxide framework. When decreasing the Al content, the strength of the residual Brönsted acid sites increases, while the number of sites decreases. At low dealumination levels, the increase in acid strength overcompensates for the loss of acid sites. In strongly dealuminated samples, the acid site strength does not increase any further upon dealumination (22, 23). This picture is, however, oversimplified, since the Al coordination chemistry in dealuminated zeolite samples is very complicated. ^{27}Al NMR has shown that there are several types of Al coordinations in the framework (24) and that a significant fraction of the framework Al atoms can change from tetrahedral to octahedral depending on temperature and atmosphere owing to hydrolysis of framework oxo bridges (25). Catalytic activity is linked with the presence of aluminum defect sites (24). In USY (Ultra-Stable Y-zeolite) samples, the aluminum concentration in individual crystals shows significant gradients (24). Several authors reported a synergetic effect of framework and extra-framework Al species in the pores. Extra-framework Al species having Lewis acid properties withdraw electron density from the bridging hydroxyl group and enhance the Brönsted acid strength. For obtaining activity enhancement, the dealumination procedure is critical (16, 18, 26–28).

In the homologous series of alkanes, the hydrocracking reactivity increases with increasing carbon number, which can be related to a stronger physisorption and the higher number of reaction possibilities of the reaction network (29). The physisorption equilibrium constant increases exponentially with the carbon number, while the reaction network expands rather linearly (11, 30).

The objective of our work was to quantify the influence of the acid strength of the zeolite and of the carbon number of the alkane reagent. For this purpose, a kinetic model on molecular level was used instead of previously used lumped or relumped models (12, 29, 30). The model was applied to an extended series of alkanes and an as-broad-as-possible variation of acidity in Pt/H–(US)Y-zeolites.

2. PROCEDURES AND MODEL EQUATIONS

2.1. Catalysts

Three zeolite samples were used (Table 1). The acidity of these samples was previously characterized using ^{27}Al MAS-NMR (24, 31), ammonium cation exchange capacity determination, and ammonia TPD (24, 31) following the method explained by Niwa *et al.* (32).

The catalysts were loaded with 0.5 wt% platinum by cation exchange with $Pt(NH_3)_4Cl_2$ in aqueous solution. They were activated in flowing oxygen, by increasing the temperature from room temperature to 673 K at 6 K/min, and keeping this temperature for 1 h. After a purge with nitrogen, the platinum was reduced in a flow of hydrogen for 1 h at 673 K. Reaction product analysis was carried out on-line with a HP 5890 gas chromatograph and a FID detector. During the experiments, no catalyst deactivation was observed.

2.2. Hydrocracking Experiments

Hydrocracking experiments were performed in a tubular flow reactor packed with catalyst pellets under the reaction conditions and with the model components mentioned in Table 2. Under these conditions "ideal" hydrocracking occurs and, hence, no differences in selectivity were observed upon altered reaction conditions (6, 29). Methane and ethane formation is indicative of the occurrence of hydrogenolysis, however, the contribution of hydrogenolysis to the observed product distributions was negligible, except for pentane on Pt/H–Y-zeolite.

TABLE 1

Zeolite H–(US)Y-Zeolite Properties

	Provider	Si/Al	Si/Al_F	C_t^a	C_t^b	C_t^c	C_{strong}^c	C_{weak}^c
				(mol kg_{cat}^{-1})				
H–Y-zeolite	Zeocat	2.6	2.6	4.6	N.D.	N.D.	N.D.	N.D.
CBV-720	PQ	14	18	0.600	0.604	0.620	0.560	0.060
CBV-760	PQ	30	60	0.217	0.365	0.235	0.189	0.046

[a] Al(IV) from quantitative ^{27}Al MAS-NMR (24, 31).

[b] Determined by cation exchange with ammonium and chemical analysis (MicroKjeldahl).

[c] Determined with ammonia TPD, weak sites: ΔH = 90–95 kJ mol^{-1}; strong sites: ΔH = 115–127 kJ mol^{-1}. The method was explained in (32); some of these data were published in (31).

TABLE 2

Catalysts, Model Components, and Range of the Experimental Conditions

	Feeds	W/F_0 (kg s mol^{-1})	X (%)	T (K)	P (MPa)	H_2/HC
Pt/H-Y	C_5–C_9,C_{12}	7–1300	0–60	506–538	0.45–0.7	13.13
Pt/CBV-720	C_6,C_9	1–36	0–40	506	0.45	13.13
Pt/CBV-760	C_5–C_9,C_{12}	4–1400	0–95	506–563	0.45–1.5	4.23–250

In the catalyst pellets of a Y-zeolite the most important mass transport resistance is located in the macropores (33). Given the similarity of particle size and porosity (34) it was assumed that the same holds for other faujasite type zeolites such as CBV-720 and CBV-760 samples considered in this work. The Weisz modulus for macropore diffusion for the Y-zeolite pellet is on the order of 10^{-3} (30).

The total conversion was calculated as

$$X_{tot} = \frac{F_{P_i,0} - F_{P_i}}{F_{P_i,0}}, \qquad [1]$$

in which i is the index corresponding with the feed component. The isomerization and cracking conversion were obtained from

$$X_{iso} = \frac{\sum_{j=I}^{n_{iso}} F_{P_j}}{F_{P_i,0}}, \qquad [2]$$

and

$$X_{cr} = X_{tot} - X_{iso}, \qquad [3]$$

with n_{iso} the number of isomers of the feed component. Due to *cracking*, the total conversion X_{tot} can amount to 100%.

2.3. Parameter Estimation

Parameter estimations were performed using a combination of a Rosenbrock (35) and a Marquardt (36) algorithm. An in-house written code was used for the Rosenbrock method, while for the Marquardt algorithm the ordinary least squares (OLS) option of the ODRPACK-package version 2.01 (37, 38) was used. Some additional source code was added to ODRPACK in order to retrieve additional statistical information.

The weighed sum of the squared differences between the observed and the calculated outlet flow rates was minimized by adjusting the model parameter vector $\boldsymbol{b}$, which is expected to approach the real parameter vector β when the optimum is reached,

$$SSQ = \sum_{k=1}^{nob} \sum_{j=1}^{nresp} w_{P_j} \left(F_{P_j,k} - \hat{F}_{P_j,k}\right)^2 \xrightarrow{\boldsymbol{b}} Min. \qquad [4]$$

The weighing factors w_{P_j} are the diagonal elements of the inverse of the covariance matrix of the experimental errors of the responses determined from replicate experiments. When no replicate experiments were available, the weighing factors were calculated from

$$w_{P_i} = \frac{\left(\sum_{k=1}^{nob} F_{P_i,k}\right)^{-1}}{\sum_{j=1}^{nresp} \left(\sum_{k=1}^{nob} F_{P_j,k}\right)^{-1}}. \qquad [5]$$

The outlet flow rates were calculated according to the model equations presented in the following two sections.

2.4. Reactor Model

The tubular flow reactor with packed catalyst bed was modeled based on a pseudohomogeneous one-dimensional model. The reactor was assumed to be fully isothermal and without any pressure drop. This leads to the following expressions for the axial flow profiles through the reactor (39)

$$\frac{dF_{P_j}}{dW} = R_{P_j} \qquad [6]$$

for all alkanes P_j but one. The axial flow profile of the remaining alkane was obtained via the atomic carbon balance. The hydrogen flow rate was calculated via the atomic hydrogen balance. The integration of the set of ordinary differential equations (ODE's) was performed with the LSODA-subroutine available at Netlib (37). It is a powerful integration routine that can handle both nonstiff and stiff sets of equations. LSODA itself has the built-in ability to decide on the stiffness of the problem and select the appropriate method, i.e., Adams and BDF methods for nonstiff and stiff problems, respectively, to integrate the set of ODE's (40, 41).

2.5. The Single Event Kinetic Model

The rate determining reaction steps were those involving C–C-bond rearrangements or breaking: alkyl-shifts, PCP branching reactions and β-scissions, viz. Fig. 1. Note that neither oligomerization nor hydride transfer had to be considered. This is justified in Appendix A. Deprotonation, protonation, and hydride shifts were considered to be in quasi-equilibrium (11).

2.5.1. Rate determining step. The reaction rate of the rate determining steps was expressed as first order in the alkylcarbenium ion intermediates

$$r_{AS/PCP/\beta}(m;n) = k_{AS/PCP/\beta}(m;n) C_{R_{i,k}^+}, \qquad [7]$$

in which $C_{R^+_{i,k}}$ represents the concentration of the reacting alkylcarbenium ion k stemming from alkane i. The rate coefficient $k_{AS/PCP/\beta}$ depends on the internal symmetry of the reactant and the activated complex, on the reaction family considered, and, within that reaction family, on the types of alkylcarbenium ions involved in that particular elementary step. The symmetry factor in the rate coefficient was taken into account via the number of single events, n_e, being the ratio between the symmetry number of the reacting alkylcarbenium ion and that of the activated complex,

$$n_e = \frac{\sigma_{R^+_{i,k}}}{\sigma_{\neq}}. \quad [8]$$

The rate coefficient in Eq. [7] could, hence, be written as

$$k_{AS/PCP/\beta}(m; n) = n_e \tilde{k}_{AS/PCP/\beta}(m; n), \quad [9]$$

where $\tilde{k}_{AS/PCP/\beta}(m; n)$ is the single event rate coefficient depending only on the reaction family and the types of alkylcarbenium ions involved. The detailed development of the single event model and the associated reduction of the number of kinetic parameters is given elsewhere (42).

2.5.2. Protonation of physisorbed alkene to physisorbed alkylcarbenium ion. The alkylcarbenium ion concentration was obtained from the alkene concentration through a Langmuir type isotherm expression

$$C_{R^+_{i,k}} = \frac{C_t K_{prot}(O_{i,j}; m) C_{o_{i,j}}}{1 + K_{prot}(O_{i,j}; m) C_{o_{i,j}}}. \quad [10]$$

The acid site coverage was calculated to be negligible, see Appendix B. Hence, Eq. [10] was simplified to

$$C_{R^+_{i,k}} \cong C_t K_{prot}(O_{i,j}; m) C_{o_{i,j}}. \quad [11]$$

Similar to the rate coefficient, the symmetry contribution in the protonation–deprotonation equilibrium coefficient was accounted for via the symmetry numbers of the alkene and the alkylcarbenium ion involved,

$$K_{prot}(O_{i,j}; m) = \frac{\sigma_{o_{i,j}}}{\sigma_{R^+_{i,k}}} \tilde{K}_{prot}(O_{i,j}; m). \quad [12]$$

The number of unknown single event protonation–deprotonation equilibrium coefficients was reduced by expressing them as the product of the single event protonation–deprotonation equilibrium coefficient of a well-chosen reference alkene O_r, $\tilde{K}_{prot}(O_r; m)$, and the single event isomerization equilibrium coefficient between the alkene $O_{i,j}$ and this reference alkene O_r, $\tilde{K}_{isom}(O_{i,j}; O_r)$, (42)

$$\tilde{K}_{prot}(O_{i,j}; m) = \tilde{K}_{isom}(O_{i,j}; O_r) \cdot \tilde{K}_{prot}(O_r; m), \quad [13]$$

so that the expression for the alkylcarbenium ion concentration becomes

$$C_{R^+_{i,k}} = C_t \frac{\sigma_{O_{i,j}}}{\sigma_{R^+_{i,k}}} \tilde{K}_{isom}(O_{i,j}; O_r) \tilde{K}_{prot}(O_r; m) C_{O_{i,j}}. \quad [14]$$

$\tilde{K}_{isom}(O_{i,j}; O_r)$ was calculated using thermodynamic data generated with Benson's group contribution method (43).

2.5.3. Dehydrogenation of a physisorbed alkane to a physisorbed alkene. Hydrogenation/dehydrogenation equilibrium expressions allowed us to relate the alkene concentration to the alkane concentration,

$$C_{O_{i,j}} = \frac{K_{deh} C_{P_i}}{p_{H_2}}, \quad [15]$$

The equilibrium coefficients for hydrogenation/dehydrogenation and isomerization were also calculated using thermodynamic data generated with Benson's group contribution method (43).

2.5.4. Physisorption of a vapor phase alkane to a physisorbed alkane. The concentration of physisorbed alkanes is calculated via a Langmuir isotherm expression,

$$C_{P_i} = \frac{C_{sat} K_{L,P_i} p_{P_i}}{I + K_{L,P_i} p_{P_i}}. \quad [16]$$

The Langmuir physisorption coefficient for an alkane on a zeolite can be determined from its Henry coefficient and saturation concentration

$$K_{L,P_i} = \frac{H_{P_i}}{C_{sat,P_i}}. \quad [17]$$

Denayer *et al.* (44) determined physisorption enthalpies and preexponential factors for the Henry coefficients using tracer chromatography, viz. Tables 3a and 3b. The saturation concentrations were taken from (45), viz. Table 3c. Since the differences in physisorption parameteres between the *n*-alkane and its isomers are negligible (33), only one set of Langmuir parameters was considered per carbon number and per Pt/H–(US)Y-zeolite.

2.5.5. Rate equations. Equations [7] to [16] ultimately lead to the following rate equation for an elementary step

$$r_{AS/PCP/\beta}(m; n) = \frac{C_{sat} K_{L,P_i} K_{deh} C_t \frac{\sigma_{O_{i,j}}}{\sigma_{R^+_{i,k}}} \tilde{K}_{isom}(O_{i,j}; O_r) \tilde{K}_{prot}(O_r; m) n_e \tilde{k}_{AS/PCP/\beta}(m; n) p_{P_i}}{\left(1 + K_{L,P_i}\right) p_{H_2}}. \quad [18]$$

The net rate of formation, $R_{R^+_{i,k}}$, of alkylcarbenium ion k, stemming from alkane i is obtained by summation of the rates of all the elementary steps in which $R^+_{i,k}$ is formed from alkylcarbenium ion o stemming from alkane l, minus

TABLE 3a

Preexponential Factors of the Henry Coefficients for the Alkanes on the H–(US)Y-Zeolites Used[a]

	C_5	C_6	C_7	C_8	C_9	C_{12}
	(mol kg_{cat}^{-1} MPa^{-1})					
H–Y-zeolite	4.2×10^{-3}	2.4×10^{-3}	1.6×10^{-3}	7.9×10^{-4}	4.5×10^{-4}	6.8×10^{-5}
CBV-720		1.4×10^{-3}			1.9×10^{-4}	
CBV-760	9.7×10^{-4}	4.6×10^{-4}	1.9×10^{-4}	9.4×10^{-5}	4.2×10^{-5}	6.5×10^{-6}

[a] Some of these data were published in (44, 45).

TABLE 3b

Physisorption Enthalpies for the Alkanes on the H–(US)Y-Zeolites Used[a]

	C_5	C_6	C_7	C_8	C_9	C_{12}
	(kJ mol^{-1})					
H–Y-zeolite	−36.1	−44.2	−50.1	−55.9	−62.0	−81.6
CBV-720		−41.9			−60.5	
CBV-760	−36.7	−43.3	−50.3	−56.5	−63.2	−81.5

[a] Some of these data were published in (44, 45).

TABLE 3c

Saturation Concentrations for the Alkanes on the H–(US)Y-Zeolites Used[a]

	C_5	C_6	C_7	C_8	C_9	C_{12}
	(mol kg_{cat}^{-1})					
H–Y-zeolite	1.50	1.29	1.22	1.07	1.02	0.691
CBV-720		0.876			0.623	
CBV-760	0.800	0.624	0.625	0.620	0.554	0.362

[a] Some of these data were published in (44, 45).

the rates of the elementary steps in which it is consumed:

$$\begin{aligned} \textit{net production} = {} & \textit{production by isomerization} \\ & - \textit{consumption by isomerization} \\ & + \textit{production by } \beta - \textit{scission} \\ & - \text{consumption by } \beta - \textit{scission} \end{aligned} \qquad [19a]$$

or

$$\begin{aligned} R_{R_{i,k}^+} = {} & \sum_l \sum_o r_{AS/PCP}(m_{l,o}; m_{i,k}) - \sum_l \sum_o r_{AS/PCP}(m_{i,k}; m_{l,o}) \\ & + \sum_l \sum_o r_\beta(m_{l,o}; m_{i,k}, O_{u,v}) \\ & - \sum_l \sum_o r_\beta(m_{i,k}; m_{l,o}, O_{u,v}). \end{aligned} \qquad [19b]$$

For clarity, the alkenes $O_{u,v}$ produced by β-scission are explicitly mentioned in Eq. [19b], although their formation is irrelevant with respect to the value of the single event rate coefficient. The net rate of formation of the alkenes j produced by β-scission stemming from alkane i is calculated as

$$R_{O_{i,j}} = \sum_l \sum_o r_\beta(m_{l,o}; m_{q,r}, O_{i,j}). \qquad [20]$$

The net rate of formation R_{P_i} of an alkane i consists of the net rates of formation of all alkylcarbenium ions stemming from alkane i and of the net rates of formation of the alkenes with the same skeletal structure formed via β-scission

$$R_{P_i} = \sum_{k=1}^{ncar_i} R_{R_{i,k}^+} + \sum_{j=1}^{nole_{i,\beta}} R_{O_{i,j}}. \qquad [21]$$

The only unknowns to be estimated in Eq. [18] by regression of kinetic data were the single event rate coefficient

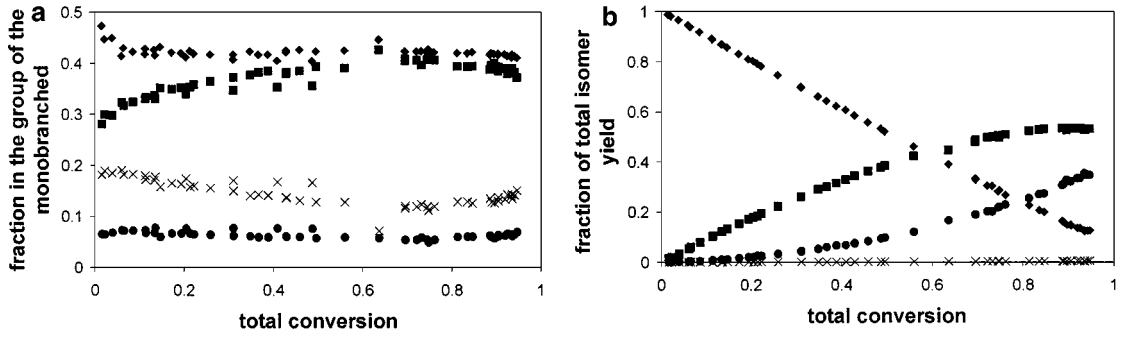

FIG. 2. Experimental distribution (a) for the group of the monobranched isomer (◆: 3-methylheptane, ■: 2-methylheptane, ●: 3-ethylhexane, ×: 4-methylheptane), (b) for all isomers classified according to their branching degree (◆: normal, ■: monobranched, ●: dibranched, ×: tribranched).

and the single event protonation–deprotonation equilibrium coefficient. Due to the low acid site coverage, viz. Eqs. [10] and [11] and Appendix B, only the product of the two can be estimated. Hence, parameter estimations based on these equations will result in composite parameters consisting of a protonation part and a contribution from the isomerization or cracking step,

$$\tilde{k}^{comp} = \tilde{K}_{prot}\tilde{k}. \qquad [22]$$

The composite activation energies represent the sum of the standard protonation enthalpy and the real activation energy,

$$E_{act}^{comp} = \Delta H_{prot}^{0} + E_{act}. \qquad [23]$$

The composite activation energy compares the energy level of the transition state and the acid site with that of the physisorbed alkene and the acid site.

The values for the composite preexponential factors were calculated according to the method explained by Martens *et al.* (12), so that the only parameters that remained to be estimated were the composite activation energies. The number of composite activation energies amounted to 12, i.e., 4 per reaction family. However, due to thermodynamic constraints the value for the (s; t) mode equals that for the (t; s) mode for the reaction family of alkyl-shift and PCP-branching (11), so that the number of parameters to be estimated was further reduced to 10.

3. RESULTS AND DISCUSSION

3.1. Hydrocracking of n-Octane on a Reference Zeolite

For alkanes with 8 carbon atoms or more, the reaction network comprises all possible isomerization and β-scission pathways. Octane was chosen as the reference component for analytical reasons. All individual skeletal isomers from C_8 could be separated by gas-chromatography. Pt/CBV-760 was selected as the reference catalyst, since it exhibits an intermediate level of activity between Pt/H-Y and Pt/CBV-720. The largest range of conversion levels was experimentally obtained with this zeolite (Table 2).

Product distributions obtained from octane hydrocracking show that from a total conversion of 20 to 30% on equilibrium is established among the group of the monobranched isomers, viz. Fig. 2a and Table 4. This indicates that alkyl shifts interconverting monobranched isomers are faster than PCP-branching reactions altering the branching degree of the isomer and faster than the β-scissions breaking the isomer into two hydrocarbon fragments. Generally stated, the same holds for the dibranched isomers. Tribranched isomers were only observed in trace amounts so that no reliable experimental distribution could be obtained. However, the 2,2,4-trimethylpentane isomer, which is the most abundant isomer under equilibrium conditions, is susceptible to fast (t; t)-β-scission and was not observed. This indicates that no equilibrium is established among the tribranched isomers. The continuous evolution in distribution between isomers with different branching degree shows that no equilibrium is established between these isomer groups. Nevertheless, at the highest conversions, the distribution between the normal and the monobranched isomers tends to equilibrium, viz. Fig. 2b and Table 4. Similar conclusions were obtained before by Vansina *et al.* (46) in a Berty reactor.

Estimations of the activation energies in the single event model for hydrocracking of octane on Pt/CBV-760 with

TABLE 4

Equilibrium Composition of the Octane Isomers at 506 K

Isomer group/individual isomer		Group fraction/individual fraction	
normal		0.09	
	2-methylheptane		0.38
	3-methylheptane		0.39
monobranched		0.44	
	4-methylheptane		0.13
	3-ethylhexane		0.10
dibranched		0.44	
tribranched		0.03	

TABLE 5

Composite Activation Energies ($\Delta H_{prot}+E_{act}$) Estimated by a Regression on the Experimental Data with *n*-Octane on Pt/CBV-760

	Alkyl shift	PCP-branching (kJ mol^{-1})	β-scission
(s;s)	16.7 (±0.1)[a]	45.6 (±0.1)	79.2 (±0.6)
(s;t)			63.7 (±4.5)
	13.7 (±2.4)	38.8 (±5.5)	
(t;s)			55.1 (±0.6)
(t;t)	7.7 (±2.9)	31.5 (±2.3)	33.9 (±1.7)

[a] 95% confidence region.

calculated preexponential factors as in (12) led to values in agreement with earlier results (11, 12), viz. Table 5. Reactions involving tertiary alkylcarbenium ions have a lower composite activation energy than those involving secondary ions. Alkyl-shifts have composite activation energies lower than PCP-branching reactions. Since the calculated preexponential factor for both reaction families is the same (12), alkyl-shifts are faster than branching rearrangements. β-scissions have the highest composite activation energies, except for the (t; t)-β-scission with a composite activation energy comparable to (t,t)-PCP-branching. However, the higher preexponential factor leads to rate coefficients that are similar to those for PCP-branching for the (s; s), (s; t) and (t; s) β-scission and an even higher rate coefficient for (t; t) β-scission than that for (t; t) alkyl-shift, viz. Table 6.

Modeling the reactor performance with the obtained kinetic parameters resulted in an adequate description of both the conversion and the selectivity ratio of isomerization to cracking (Fig. 3). The same holds for the outlet flow rates of isomers and cracked products (Fig. 4).

3.2. Effect of Carbon Number on Alkene Protonation Enthalpy

An increased reactivity with the carbon number was observed in the range of C_5 to C_9, whereas for C_{12} a slight decrease in reactivity with respect to C_9 was observed (Fig. 5a). The increased reactivity of heavier alkanes in the range C_5–C_9 can be attributed to their stronger physisorption and their more extended set of reaction possibilities. The decrease in reactivity from C_9 to C_{12} was caused by physisorption saturation effects. Physisorbed nonanes and dodecanes are at relatively 84 and 98% of their saturation concentration. From the saturation concentrations mentioned in Table 3c it is clear that the concentration of physisorbed nonanes is higher than of the physisorbed dodecanes.

According to the single-event model, the carbon number effect on the reaction kinetics is entirely due to physisorption and reaction network effects. In the model, the protonation–deprotonation equilibrium of the reference alkene (2-methyl-2-alkene) is assumed only to depend on the type of alkylcarbenium ion and not on the carbon number,

$$K_{prot}(O_r; m) = K_{prot}(m). \qquad [24]$$

The alkylcarbenium ion stability *according to the model* depends on the number of α C–C bonds (11, 12, 42). Methyl and primary alkylcarbenium ions were assumed to be too unstable. Only two types of alkylcarbenium ions were considered, having a different stability, i.e., secondary and tertiary ions. For example, according to the model the stability of the 3-octyl cation is identical to that of the 2,2,4-trimethyl-3-pentyl cation.

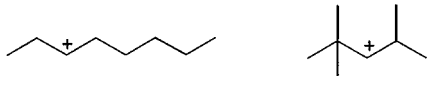

These two cations have 2 α C–C bonds. However, the 2,2,4-trimethyl-3-pentyl cation has 3 β C–C bonds more than the 3-octyl cation, resulting in a difference in stability of these two cations in the gas phase of a few kJ mol^{-1} (47, 48). The model used considers no differences in stability between these two cations on the catalyst surface. Hence, the estimated composite activation energies (Eq. 23) are based on an average value of the standard protonation enthalpy. The independence of the single event rate parameters on the carbon number implies that this average level is independent of the carbon number.

In the model both the intermediate and the activated complex of acid-catalyzed steps were considered to have ionic character. The effect of the carbon number on the stability of the intermediate and the activated complex were expected to be the same. Hence, the activation energy is independent of the carbon number (Fig. 6). Consequently, the carbon number effect on the composite activation energy could be entirely attributed to an effect on the standard protonation enthalpy, so that Eq. [23] could be written as

$$\Delta_{CN_j-CN_i}\left(E_{act}^{comp}\right) = \Delta_{CN_j-CN_i}\left(\Delta H_{prot}^{0}\right). \qquad [25]$$

TABLE 6

Composite Rate Coefficients ($K_{prot}(O_r; m)k(m; n)$) at 506 K Obtained with the Estimated Composite Activation Energies and the Preexponential Factors Calculated as in (12)

	Alkyl shift	PCP-branching (kg_{cat} mol^{-1} s^{-1})	β-scission
(s;s)	9.9×10^6	10.3×10^3	3.9×10^3
(s;t)			153×10^3
	20.2×10^6	52.0×10^3	
(t;s)			1.2×10^6
(t;t)	84.2×10^6	295×10^3	183×10^6

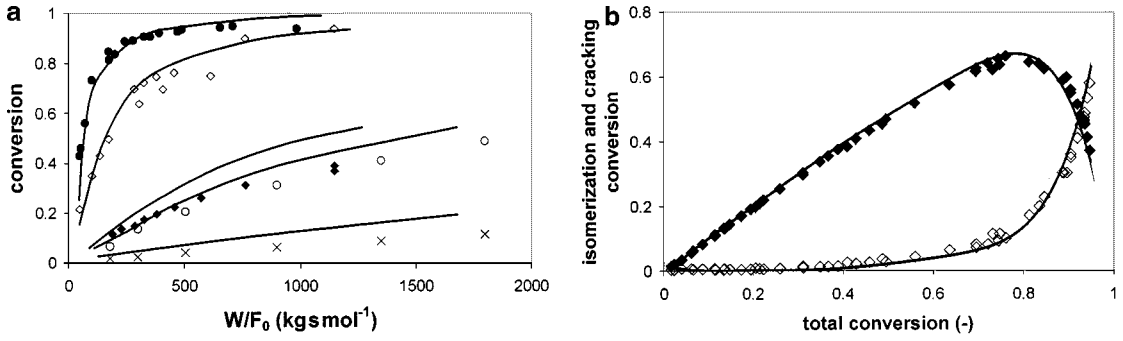

FIG. 3. Experimental (symbols) and calculated (lines) results for (a) C_8 conversion on Pt/CBV-760 as a function of space time (◆: 506 K – 0.45 MPa – H_2/HC = 13.13, ◇: 539 K – 0.45 MPa – H_2/HC = 13.13, ●: 563 K – 0.45 MPa – H_2/HC = 13.13, ○: 539 K – 0.7 MPa – H^2/HC = 250, × : 506 K – 0.7 MPa – H_2/HC = 250) and for (b) C_8 selectivity on Pt/CBV-760 to isomers (◆) and cracked products (◇). The calculated results have been obtained using Eqs. [7]–[21] with the estimated composite activation energies from Table 5 and the preexponential factors calculated as in (12).

Differences in standard protonation enthalpy on the zeolite were related to differences in standard protonation enthalpy in the gas phase by considering the Born–Haber cycle in Fig. 7,

$$\Delta H^0_{prot,zeo} = \Delta H^0_{stab,R^+} + \Delta H^0_{prot,gas} - \Delta H^0_{stab,H^+} - \Delta H^0_{phys,O}. \quad [26]$$

In Eq. [26] $\Delta H^0_{stab,H^+}$ is carbon number independent. The carbon number dependence of $\Delta H^0_{phys,O}$ is related to differences in alkene physisorption, while that of $\Delta H^0_{stab,R^+}$ consists of two contributions,

$$\Delta_{CN_j-CN_i}\left(\Delta H^0_{stab,R^+}\right) = \Delta_{CN_j-CN_i}\left(\Delta H^0_{phys,R^+}\right) + \Delta_{CN_j-CN_i}\left(\Delta H^0_{chem,R^+}\right). \quad [27]$$

In Eq. [27] $\Delta H^0_{phys,R^+}$ accounts for physical interactions with the zeolite pores, i.e., physisorption, while $\Delta H^0_{chem,R^+}$ accounts for electrostatic interactions of the alkylcarbenium ion with a deprotonated acid site. The effect of the carbon

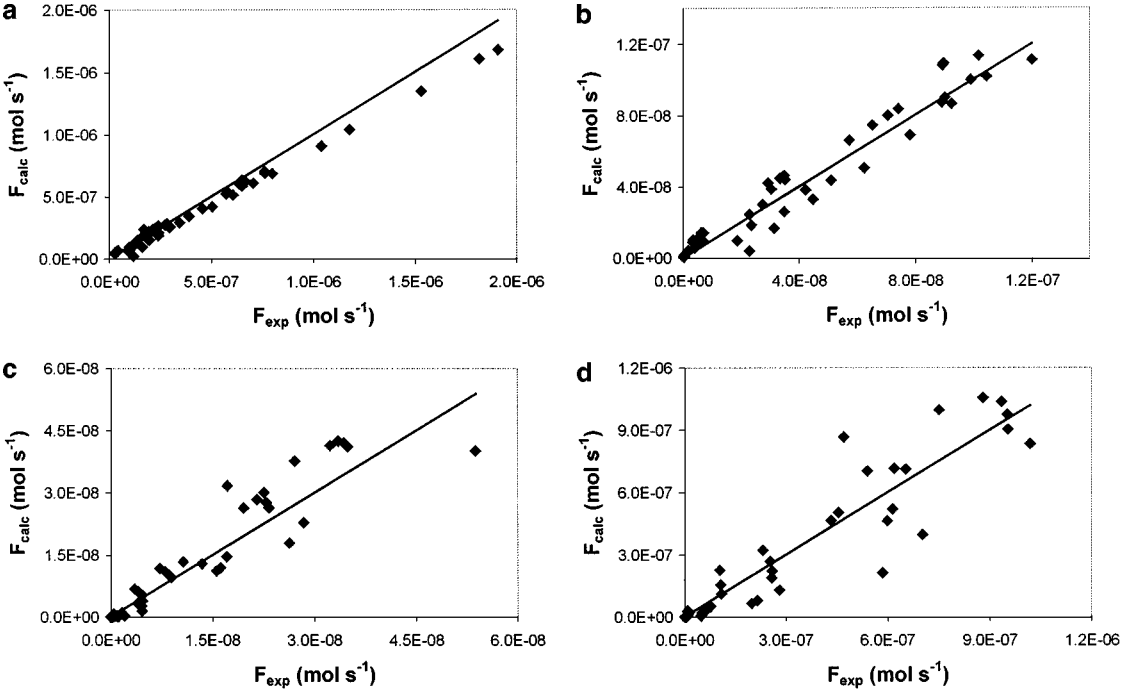

FIG. 4. Parity diagrams for the outlet flow rates for some typical hydrocracking products from octane on Pt/CBV-760 (a) 3-methyl-heptane, (b) 3, 3-dimethyl-hexane, (c) *n*-pentane, and (d) isobutane. Range of experimental conversions, viz. Table 2. The calculated outlet flow rates have been obtained using Eqs. [7]–[21] with the estimated composite activation energies from Table 5 and the preexponential factors calculated as in (12).

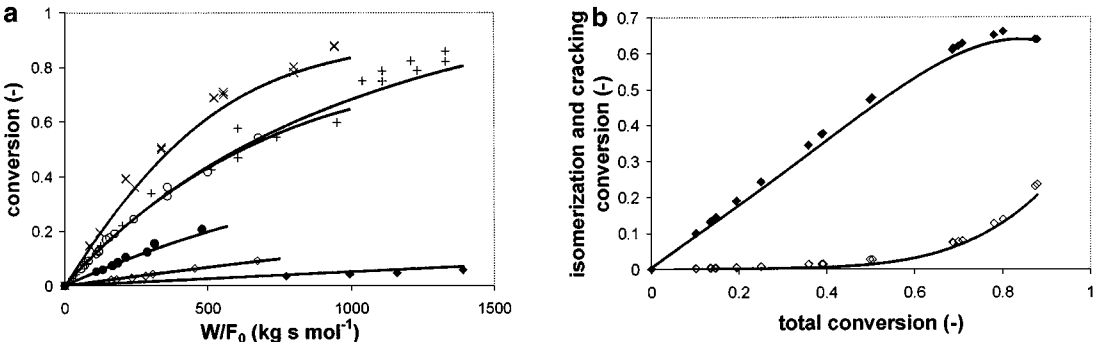

FIG. 5. Experimental (symbols) versus calculated (lines) results for (a) alkane conversion on Pt/CBV-760 as a function of space time at 506 K − 0.45 MPa − H_2/HC = 13.13 (except for pentane at 539 K) (◆: pentane, ◇: hexane, ●: heptane, ○: octane, ×: nonane, +: dodecane) and for (b) nonane selectivity to isomers (◆) and cracked products (◇). The calculated outlet flow rates have been obtained using Eqs. [7]–[21] with the estimated composite activation energies from Table 5 and the preexponential factors calculated as in (12).

number on $\Delta H^0_{phys,R^+}$ is expected to be similar to the effect of the carbon number on $\Delta H^0_{phys,O}$,

$$\Delta_{CN_j-CN_i}\left(\Delta H^0_{phys,R^+}\right) \cong \Delta_{CN_j-CN_i}\left(\Delta H^0_{phys,O}\right). \quad [28]$$

The expression for the standard protonation enthalpy increase for a hydrocarbon with carbon number CN_j with respect to the reference hydrocarbon with carbon number CN_i can then be written as

$$\Delta_{CN_i-CN_j}\left(\Delta H^0_{prot,zeo}\right) = \Delta_{CN_i-CN_j}\left(\Delta H^0_{prot,gas}\right) + \Delta_{CN_i-CN_j}\left(\Delta H^0_{chem,R^+}\right). \quad [29]$$

For two alkenes with different carbon number, Eq. [29] represents the sum of the difference in gas phase standard protonation enthalpy and the difference in stabilization enthalpy by electrostatic interactions of the alkylcarbenium ion with the deprotonated acid site. A similar equation for the carbon number dependence of the standard protonation enthalpy can be obtained via the concept of the "proton transfer energy" Q_p as used by van Santen and Kramer (23) to describe the protonation of a gas phase alkene by an acid site,

$$Q_p = -PA^{base}_{gas} + PA^{acid}_{solid} + E_{zi}, \quad [30]$$

in which PA^{base}_{gas} stands for the proton affinity of the gas phase carbenium ion, which is equal to $-\Delta H^0_{prot,gas}$. PA^{acid}_{solid} is defined as the proton affinity of a surface hydroxyl and E_{zi} is the Zwitterion stabilization energy between the protonated base, i.e., the alkylcarbenium ion, and the negatively charged zeolite wall, i.e., the deprotonated acid site. E_{zi} equals the stabilization enthalpy of the carbenium ion due to electrostatic interactions with the deprotonated acid site. $\Delta H^0_{chem,R^+}$. The carbon number dependence of Q_p contains two contributions,

$$\Delta_{CN_i\text{-}CN_j}(Q_p) = \Delta_{CN_i\text{-}CN_j}\left(-PA^{base}_{gas}\right) + \Delta_{CN_i\text{-}CN_j}(E_{zi}), \quad [31]$$

which can be identified with the two terms in Eq. [29].

The values of the standard protonation enthalpy increase for the investigated alkenes with respect to C_8-alkenes were estimated by regression of experimental hydrocracking data on Pt/CBV-760. This was done keeping the previously determined values of the composite activation energies

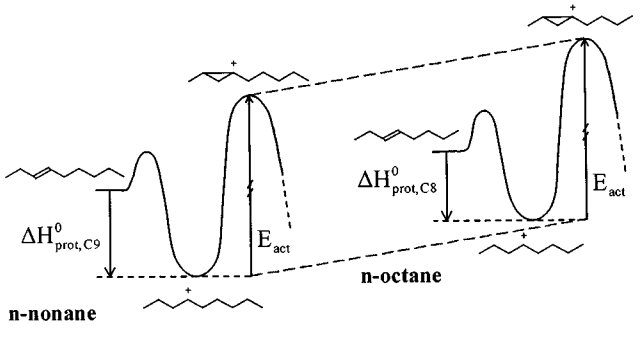

FIG. 6. Energy levels for the intermediates in an elementary acid-catalyzed step, effect of the carbon number of the intermediate.

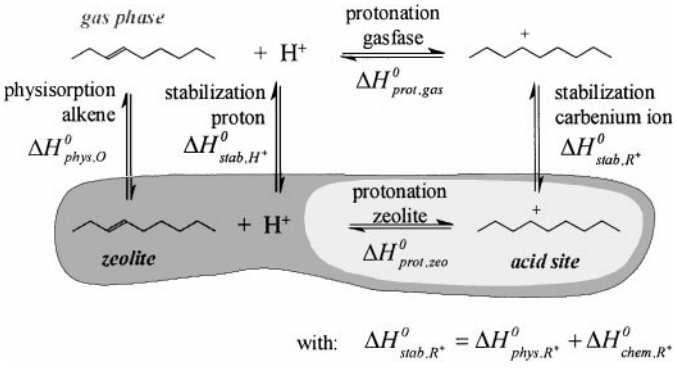

FIG. 7. Born–Haber cycle relating the standard protonation enthalpy on the zeolite with the gas phase protonation enthalpy.

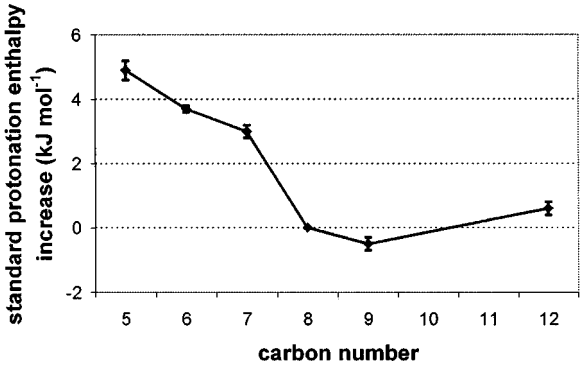

FIG. 8. Standard protonation enthalpy increases on Pt/CBV-760 as a function of the carbon number (reference: octane).

fixed for alkyl-shift, PCP-branching, and β-scission. The effect of the carbon number on the physisorption is taken into account via the physisorption properties (Eq. [18], Tables 3a–3c). The extension of the reaction network is apparent from the summations in Eqs. [19] to [21].

Estimations of the standard protonation enthalpy increase for the various model components resulted, similar to the reference case, in satisfactory description of the total conversion and of the selectivity to isomers and cracked products (Fig. 5). The outlet flow rates of the individual components were adequately described. The estimated values for the standard protonation enthalpy first increase, then decrease, and subsequently level out with increasing carbon number (Fig. 8). A set of data obtained on one catalyst batch leads to a typical error on the standard protonation enthalpy increase of 0.5 kJ mol^{-1}. However, a set of data obtained on several catalyst batches has an error of 1 to 1.5 kJ mol^{-1}. The increments with carbon number vary from -3 to less than -1 kJ mol^{-1}, which is in the order of magnitude expected when β C–C bonds are invoked to explain differences in the alkylcarbenium ion stability. The significant variations at lower carbon numbers originate from the more pronounced inductive effects of alkyl-substituents in the C_5–C_8 range compared to heavier components, i.e., C_8–C_{12}. According to the error obtained on several catalyst batches, no significant variations are observed for the heavier components. The leveling out from carbon numbers of 8 on is also in agreement with previous modeling work (12) and supports the carbon number independence of the single event kinetic parameters for C_8 and heavier hydrocarbons.

3.3. Effect of Average Catalyst Acid Strength on Alkene Protonation Enthalpy

Experimentally, only differences in activity but not in selectivity were observed when feeding the same alkane over the three Pt/H–(US)Y-zeolites with different average acid strengths. This is illustrated in Fig. 9 for nonane. Similar results were obtained for hexane on the three zeolites and for the other alkanes on Pt/H–Y and Pt/CBV-760. The absence of selectivity differences indicates that all the rate determining steps were influenced to a same extent upon variation of the average acid strength of the zeolite.

The intermediate and the activated complex in these acid-catalyzed reactions were assumed to have ionic character. Hence, the acid strength of an active site will influence the stability of both species. It can reasonably be assumed that the relative stability of the intermediate and the activated complex is independent of the acid strength and, hence, that the activation energy is not depending on the acid strength. Therefore, the difference in activity can be attributed to a difference in standard protonation enthalpy of the alkenes on the zeolite (Fig. 10).

The physical meaning of the standard protonation enthalpy of alkenes, Eq. [26], is given in Fig. 7. The acid strength dependence of $\Delta H^0_{stab,R^+}$ can be split up into an electrostatic and a physical contribution, Eq. [27]. The differences in physisorption of alkylcarbenim ions between two zeolite samples were taken as the differences

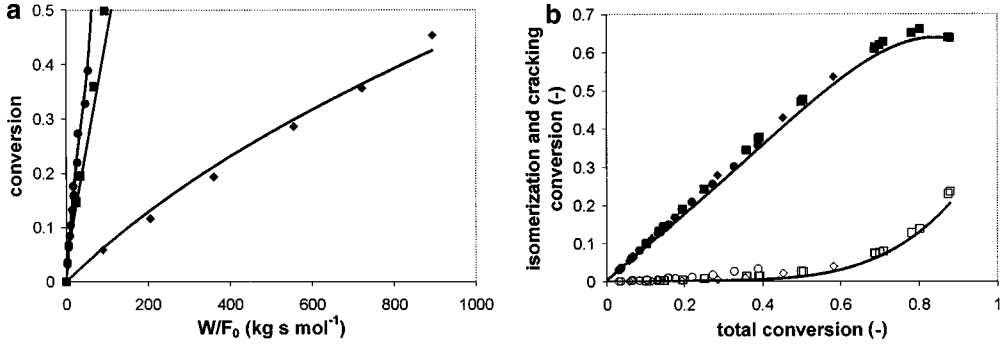

FIG. 9. Experimental (symbols) versus calculated (lines) results for (a) nonane conversion as a function of space–time at 506 K – 0.45 MPa – H_2/HC = 13.13 and for (b) nonane selectivity to isomers (closed symbols) and cracked products (open symbols) (◆: Pt/H–Y-zeolite, ●: Pt/CBV-720, ■: Pt/CBV-760). The calculated outlet flow rates have been obtained using Eqs. [7]–[21] with the estimated composite activation energies from Table 5 and the preexponential factors calculated as in (12).

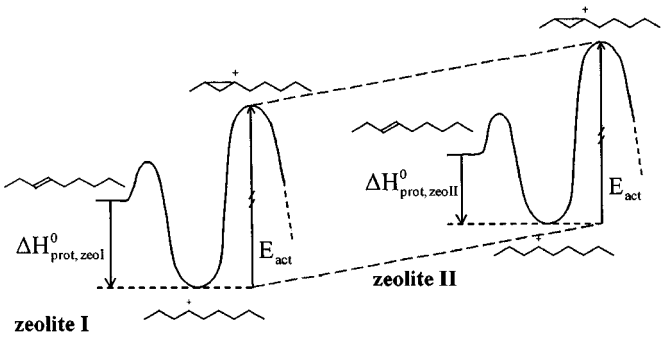

FIG. 10. Energy levels for the intermediates in an elementary acid-catalyzed step, effect of the acid strength of the active site.

in physisorption between the corresponding alkenes,

$$\Delta_{zeo_{II}-zeo_I}\left(\Delta H^0_{phys,R^+}\right) \cong \Delta_{zeo_{II}-zeo_I}\left(\Delta H^0_{phys,O}\right). \quad [32]$$

Following these considerations, the standard protonation enthalpy increase for an alkene on a Pt/H–(US)Y-zeolite with respect to a reference Pt/H–(US)Y-zeolite can be written as

$$\Delta_{zeo_{II}-zeo_I}\left(\Delta H^0_{prot,zeo}\right) = \Delta_{zeo_{II}-zeo_I}\left(\Delta H^0_{chem,R^+}\right) - \Delta_{zeo_{II}-zeo_I}\left(\Delta H^0_{stab,H^+}\right). \quad [33]$$

Similar to the case of the carbon number effect, an equation analogous to Eq. [33] can be derived via the so-called proton transfer energy Q_p. The two acid strength dependent contributions in Q_p

$$\Delta_{zeo_{II}-zeo_I}(Q_p) = \Delta_{zeo_{II}-zeo_I}\left(PA^{acid}_{solid}\right) + \Delta_{zeo_{II}-zeo_I}(E_{zi}) \quad [34]$$

can be identified with the two terms in Eq. [33], i.e., PA^{acid}_{solid} with the $-\Delta H^0_{stab,H^+}$ and E_{zi} with $\Delta H^0_{chem,R^+}$. Other groups (21, 49–53) made similar considerations on the effect of the acid strength based on the work of Dumesic *et al.* (54). Those authors related gas phase reference data to the zeolite considered by the definition of a ΔH^+, which represents the stabilization enthalpy of the alkylcarbenium ion by the zeolite, relative to the stabilization enthalpy of a proton by the zeolite. The standard protonation enthalpy increase as expressed in Eq. [33] is equal to the difference between the two ΔH^+-values for the respective zeolites,

$$\Delta_{zeo_{II}-zeo_I}\left(\Delta H^0_{prot,zeo}\right) = \Delta H^+_{zeo_{II}} - \Delta H^+_{zeo_I}. \quad [35]$$

The effect of the acid strength on the hydrocracking behavior was investigated by modeling the hydrocracking experiments with nonane on three Pt/H–(US)Y-zeolites. The standard protonation enthalpy increases of the nonenes on the Pt/H–(US)Y-zeolites with respect to the nonenes on the reference Pt/H–USY-zeolite, Pt/CBV-760, were estimated, keeping the values of the composite activation energies fixed at the values in Table 5. Differences in physisorption properties of nonane were taken into account via C_{sat} and K_{L,P_i} in Eq. [18] (Tables 3a–3c).

The obtained results for each of the Pt/H–(US)Y-zeolites are interpreted in terms of a single acid site strength for each zeolite. In reality, Pt/H–(US)Y-zeolites have an acid strength distribution (Table 1), so that the single one acid strength reported, represents an average acid strength. Since the acid site coverage is low (Appendix B) the average acid strength of only the strongest acid sites is considered. The substitution of the acid strength distribution by a single average acid strength has no effect on the reaction rate of an elementary acid catalyzed step calculated with the single event model.

The only acid strength dependent parameter in Eq. [18] for the rate of an elementary acid catalyzed step is the single event protonation–deprotonation equilibrium coefficient. Using the standard protonation enthalpy of the alkene on the acid site for the quantification of the acid strength of the site, a normalized acid strength distribution $E_{distr}(\Delta H^0_{prot})$ can be introduced (55),

$$\int_{\Delta H^{0,lower}_{prot}}^{\Delta H^{0,upper}_{prot}} E_{distr}\left(\Delta H^0_{prot}\right) d\left(\Delta H^0_{prot}\right) = 1. \quad [36]$$

The reaction rate on the Pt/H–(US)Y-zeolite of an elementary step equals the sum of the reaction rates on each active site. Considering a continuous distribution, an integration rather than a summation is performed,

$$r_{AS/PCP/\beta} = \int_{\Delta H^{0,lower}_{prot}}^{\Delta H^{0,upper}_{prot}} r_{AS/PCP/\beta}\left(\Delta H^0_{prot}\right) E_{distr}\left(\Delta H^0_{prot}\right) d\left(\Delta H^0_{prot}\right). \quad [37]$$

By selection of a reference value for ΔH^0_{prot}, the reaction rate on an active site can be written as

$$r_{AS/PCP/\beta}\left(\Delta H^0_{prot}\right) = r_{AS/PCP/\beta}\left(\Delta H^{0,ref}_{prot}\right) \exp\left(-\frac{\Delta H^0_{prot} - \Delta H^{0,ref}_{prot}}{R\,T}\right), \quad [38]$$

so that Eq. [37] becomes,

$$r_{AS/PCP/\beta} = r_{AS/PCP/\beta}\left(\Delta H^{0,ref}_{prot}\right) \exp\left(\frac{\Delta H^{0,ref}_{prot}}{R\,T}\right) \times \int_{\Delta H^{0,lower}_{prot}}^{\Delta H^{0,upper}_{prot}} \exp\left(-\frac{\Delta H^0_{prot}}{R\,T}\right) E_{distr}\left(\Delta H^0_{prot}\right) d\left(\Delta H^0_{prot}\right). \quad [39]$$

In Eq. [39] the integral equals the mean value of $\exp(-\Delta H^0_{prot}/RT)$ from which an average value of ΔH^0_{prot} can be determined so that the final equation for the total reaction rate of an acid catalyzed elementary step becomes

$$r_{AS/PCP/\beta} = r_{AS/PCP/\beta}\left(\Delta H^{0,ref}_{prot}\right) \times \exp\left(-\frac{\Delta H^{0,ave}_{prot} - \Delta H^{0,ref}_{prot}}{RT}\right). \quad [40]$$

Equation [40] clearly shows that working with $\Delta H^{0,ave}_{prot}$ or explicitly taking into account the acid strength distribution of the zeolite leads to identical model predictions owing to the nature of the model equations.

The total hydrocracking conversion, the isomerization and the cracking conversion of nonane on the three zeolites (Fig. 9), and the individual outlet flow rates were simulated satisfactoraly. The estimated standard protonation enthalpy increases for the three zeolites, ordered according to their Si/Al-ratio is shown in Fig. 11. The highest value of the standard protonation enthalpy increase, corresponding with the weakest average acid strength, was found for the Pt/H–Y-zeolite, as expected. In the dealuminated Pt/CBV-720 sample, the standard protonation enthalpy was lower, reflecting the increase of average acid strength (Fig. 11). Moreover, the standard protonation enthalpy increase for Pt/CBV-720 was lower than that of the most dealuminated Pt/CBV-760 sample. Consequently, the average acid strength of Pt/CBV-720 was slightly higher than that of Pt/CBV-760. This decrease of the acid strength at very high dealumination levels is in agreement with the commonly observed trends commented in the Introduction.

3.4. Combined Effect of Carbon Number and Acid Strength

A series of experiments with alkanes ranging from C_5 to C_{12} have been performed on the Pt/H–Y-zeolite, so that both the carbon number and the zeolite were different from the reference case, i.e., octane on Pt/CBV-760. The relative reactivities observed were similar to those for the series of alkanes on Pt/CBV-760; however, the absolute reactivity on the Pt/H–Y-zeolite was much lower. Estimates for the standard protonation enthalpy increase with respect to the reference case were obtained by regression of the corresponding kinetic data, maintaining all the kinetic parameters related to the carbenium ion rearrangements fixed at their reference values. These estimates account simultaneously for the effect of the carbon number, viz. Eq. [29], Section 3.2, and the effect of the average acid strength, viz. Eq. [33], Section 3.3. By comparison with the sum of the values obtained while investigating the two effects separately (Eqs. [29] and [33]), the additivity of the latter was verified. The altered physisorption behavior was taken into account via C_{sat} and K_{L,P_i} in Eq. [18] (Tables 3a–3c).

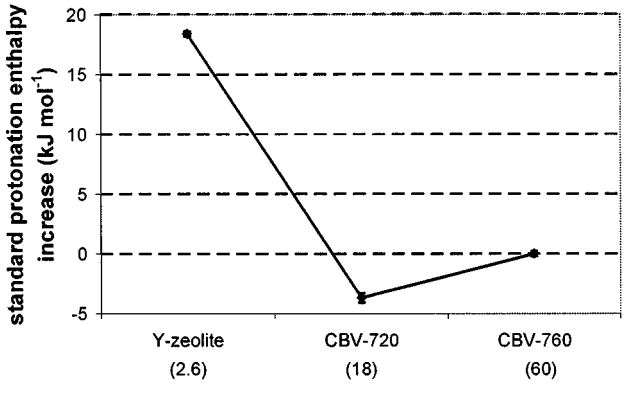

FIG. 11. Standard protonation enthalpy increase for nonane on three Pt/H–(US)Y-zeolites (reference Pt/CBV-760).

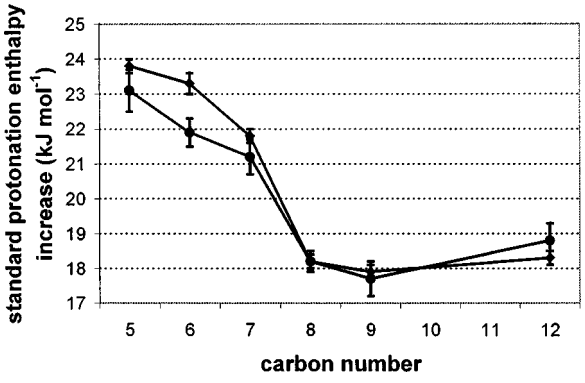

FIG. 12. Standard protonation enthalpy increases for alkanes on Pt/H–Y-zeolite (reference: octane on Pt/CBV-760). Direct estimation for the combined effect of carbon number and acid strength (◆) compared to the sum of the results for the two separate effects (●).

A good agreement between experimental and calculated total hydrocracking conversion and isomerization and cracking conversion was observed as well as for the individual outlet flow rates. The estimated values for the standard protonation enthalpy increases are shown in Fig. 12 and compared with the sum of the two separate effects. Additivity, within the statistical limits, was observed for all the alkanes used in this work, except for hexane. However, since the deviation found for hexane does not further increase, but even decreases when pentane is considered, it can be stated that the standard protonation enthalpy increase with the carbon number is independent of the zeolite considered.

The high values for the standard protonation enthalpy increase on the Pt/H–Y-zeolite reflect how difficult acid catalyzed alkane activation occurs on Pt/H–Y-zeolite. Hence, other reaction pathways, such as hydrogenolysis, can become dominant. The difficult alkane activation on Pt/H–Y-zeolite was most obvious for pentane, where hydrogenolysis accounted for about half of the pentane conversion. The average acid strength of a Pt/H–Y-zeolite is too weak for pentene protonation.

4. CONCLUSIONS

The effect of reactant carbon number and average acid strength of zeolites on the hydrocracking activity was investigated via the kinetic modeling of alkane hydrocracking data on three Pt/H–(US)Y-zeolites. Physisorption was explicitly accounted for based on independently obtained information.

The effect of the reactant carbon number was incorporated in the model through the introduction of the standard protonation enthalpy of physisorbed alkenes as the only parameter. The estimated standard protonation enthalpies indicate a stabilization of the carbenium ions which increases with the carbon number in the range C_5 to C_8. The latter is caused by an increase of branching possibilities allowing extra inductive stabilization. For carbon numbers of C_8 and larger, the effect levels out. The carbon number effect on the standard protonation enthalpy is independent of the zeolite.

The standard protonation enthalpy of alkenes also offers a means to quantify the average acid strength of Pt/H–(US)Y-zeolites. Accounting for different average acid strengths could also be achieved by adjustment of the standard protonation enthalpy. The estimated values show a shallow maximum in average acid strength for the Pt/CBV-720 sample, while the average acid strength of Pt/H–Y-zeolite is too weak for pentene protonation.

APPENDIX A

Considerations on Oligomerization and Hydride Transfer

A.1. Oligomerization

Oligomerization, as a bimolecular reaction, depends on the concentration of both the carbenium ions and the alkenes,

$$O_{C1} + R^+_{C2} \leftrightarrow R^+_{C1+C2}.$$

The affinity of a reaction measures how strong the oligomerization reaction deviates from equilibrium and is an indication of which reaction is dominating, the forward ($A_r \gg 0$) or the reverse ($A_r \ll 0$).

$$\frac{r_{forward}}{r_{reverse}} = \exp\left(\frac{A_r}{RT}\right).$$

Taking into account the equilibrium of the (de)hydrogenation and (de)protonation reactions, the affinity for the oligomerization reaction can be written as a function of hydrogen and alkane partial pressures:

$$A_r = RT\ ln\, K \frac{p_{P_{C1}} p_{P_{C2}}}{p_{P_{C1+C2}} p_{H_2}}.$$

Under the present conditions of temperature, pressure, and molar hydrogen to hydrocarbon ratio and for a feed molecule conversion of 99% a value $A_r = -35 \times 10^3$ J mol^{-1} is found corresponding to a ratio of the forward, oligomerization, to the reverse, cracking, reaction rate of 0.25×10^{-3}. Hence, even at 99% conversion, cracking proceeds more than 1000 times faster than oligomerization, justifying the neglect of oligomerization reactions in the reaction network.

A.2. Hydride Transfer

In the hydrocracking model, hydride transfer is kinetically insignificant. Since only ideal hydrocracking experiments are considered (equilibrated metal catalyzed reactions) and since the protonation of the alkenes can be assumed to be in equilibrium, equilibrium is established between a carbenium ion and a corresponding alkane. This means that for a hydride transfer,

$$P_1 + R^+_2 \rightleftharpoons R^+_1 + P_2,$$

the alkane P_1 is in equilibrium with carbenium ion R^+_1 and the carbenium ion R^+_2 is in equilibrium with alkane P_2. Hence, the molecules involved in hydride transfer are in equilibrium and the eventual occurrence of a slower, rate-determining hydride transfer can be neglected compared to the fast (de)hydrogenation and (de)protonation. Moreover, comparing the reaction rate for hydride transfer with typical rates for acid-catalyzed reactions such as for isomerization or cracking, a reaction rate for hydride transfer at 500 K more than 600 times slower than for the slowest isomerization or cracking steps at 500 K is found (56). Hence, it is expected that even when (de)hydrogenation and/or (de)protonation are not equilibrated, the rate of the rate- determining steps in hydrocracking will still be significantly faster than the rate of hydride transfer.

APPENDIX B

Acid Site Coverage

The energy levels involved in this calculation are schematically shown in Fig. B-1. Under the typical reaction

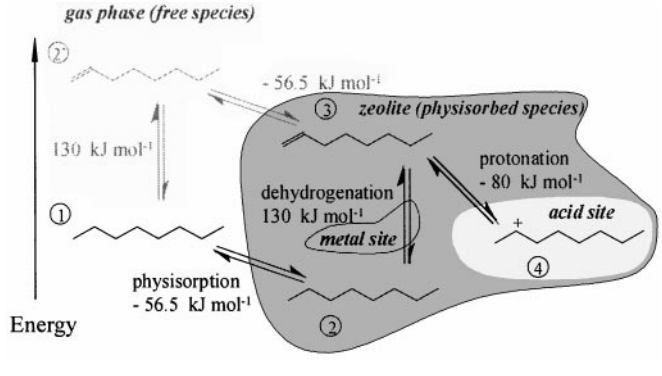

FIG. B-1. Schematic representation of the energy levels involved in alkylcarbenium ion formation.

conditions mentioned in Table 2 the alkane and hydrogen partial pressure amount to 0.032 MPa and 0.418 MPa. From this alkane (Fig. B-1, level 1) partial pressure, the corresponding physisorbed alkane (Fig. B-1, level 2) concentration can be calculated according to a Langmuir isotherm. Henry coefficients and saturation concentrations are available (33, 45), so that the Langmuir coefficient for a typical alkane such as octane, can be calculated,

$$K_{L,C_8} = 103 \text{ MPa}^{-1} \quad [1]$$

with which the physisorbed alkane concentration becomes

$$C_{C_8} = 0.476 \text{ mol kg}_{\text{cat}}^{-1}. \quad [2]$$

Based on the enthalpies of formation and the absolute entropies of octane, 1-octene, and hydrogen a value for the dehydrogenation equilibrium coefficient was calculated at 506 K:

$$K_{deh} = 0.5019\,10^{-7} \text{ MPa}. \quad [3]$$

Based on these values the concentration of physisorbed alkenes (Fig. B-1, level 3) amounts to

$$C_{C_8^=} = 5.72\,10^{-8} \text{ mol kg}_{\text{cat}}^{-1}. \quad [4]$$

A value for the protonation–deprotonation equilibrium coefficient is not directly available, but a reasonable estimate can be made. The protonation entropy is calculated according to Martens *et al.* (12) and amounts to -67 J mol^{-1} K^{-1}. For the standard protonation enthalpy, values are at hand from quantumchemical calculations (7). These involve the formation of a σ-bond between the alkene and the active site and, hence, will result in a more negative value for the protonation enthalpy than when an ionic bond is considered. However, in an attempt to calculate the standard protonation enthalpy corresponding with the formation of carbenium ions, Martens *et al.* (12) arrived at values of -120 and -150 kJ mol^{-1} for secondary and tertiary carbenium ions, respectively. These values are lower than that obtained via direct quantumchemical calculations, i.e., -80 kJ mol^{-1}. They were based on an indirect method, incorporating estimated, tabulated, and quantumchemically calculated values and is therefore thought to be less reliable. Hence, the surface concentration of carbenium ions calculated based on the directly quantumchemically obtained value, is considered as an upper limit. The equilibrium coefficient becomes

$$K_{prot} = 57400 \text{ kg}_{\text{cat}} \text{ mol}^{-1}.$$

This protonation coefficient provides the link between the concentration of the physisorbed alkenes and the (physisorbed) carbenium ions. It only comprises the formation of an ionic center from a double bond. The van der Waals interactions of the other carbon atoms with the zeolite wall are taken into account via the physisorption coefficient.

The upper limit for the carbenium ion (Fig. B-1, level 4) concentration amounts to

$$C_{R^+_{tot}} = 7.1010^{-4} \text{ mol kg}_{\text{cat}}^{-1}.$$

Compared with the minimum total concentration of acid sites of 0.217 mol kg$_{\text{cat}}^{-1}$, viz. Table 1, this maximum concentration of carbenium ions is negligible, justifying the assumption of low acid site coverage.

APPENDIX C: NOMENCLATURE

Roman Symbols

AS	Alkyl-Shift
b	model parameter vector containing the estimated parameter values
C	concentration [mol kg$_{\text{cat}}^{-1}$]
C_t	total concentration of acid sites [mol kg$_{\text{cat}}^{-1}$]
CN	carbon number
E	energy [J mol^{-1}]
E_{distr}	distribution function
F	molar flow rate [mol s^{-1}]
H	Henry coefficient [mol kg$_{\text{cat}}^{-1}$ MPa^{-1}]
ΔH^+	stabilization enthalpy of the carbenium ion by the zeolite relative to that of the proton [J mol^{-1}]
ΔH^0	standard reaction enthalpy [J mol^{-1}]
HS	Hydride-Shift
j	index
K_{deh}	equilibrium coefficient for dehydrogenation [MPa]
$K_{isom}(O_{i,j}; O_r)$	equilibrium coefficient for isomerization between alkene j and the reference alkene [$-$]
K_L	Langmuir physisorption coefficient [MPa^{-1}]
$K_{prot}(O_{i,j}; m)$	equilibrium coefficient for protonation of alkene j with formation of a carbenium ion of type m [kg$_{\text{cat}}$ mol^{-1}]
$k(m; n)$	rate coefficient of a reaction converting a carbenium ion of type m into another carbenium ion of type n [s^{-1}]
k	index
m	carbenium ion type (secundary or tertiary)
n	carbenium ion type (secundary or tertiary)
n	number of components
n_e	number of single events
$ncar$	number of carbenium ions
nob	number of observations
$nole$	number of alkenes
$nresp$	number of responses
$O_{i,j}$	alkene j stemming from alkane i

P_i	alkane *i*
PA	proton affinity [J mol^{-1}]
PCP	Protonated Cyclo-Propane
p	partial pressure [MPa]
Q_p	proton transfer energy [J mol^{-1}]
R	net production rate [mol (kg s)$^{-1}$]
$R^+_{i,k}$	carbenium ion k stemming from alkane i
$r(m;n)$	rate of a reaction converting a carbenium ion of type m into another carbenium ion of type n [mol (kg s)$^{-1}$]
SSQ	sum of squares
w	response weighing factor
X	conversion

Greek Symbols

β	β-scission
β	model parameter vector containing the real parameter values
σ	symmetry number

Superscript

$\wedge$	model calculated value
$\sim$	single event
ave	average
comp	composite
ref	reference

Subscript

$\neq$	transition state
0	inlet
act	activation
cat	catalyst
chem	chemical
cr	cracking
deh	dehydrogenation
i	component number
iso	isomerization
phys	physisorption, physical
prot	protonation
r	reference
sat	saturation
stab	stabilization
tot	total
zeo	zeolite
zi	Zwitter ion

ACKNOWLEDGMENT

This research was carried out in the framework of "Interuniversity Attraction Poles," funded by the Belgian government and the DWTC office.

REFERENCES

1. Ward, J. W., *Stud. Surf. Sci. Catal.* **53**, 417 (1989).
2. Ward, J. W., *Fuel Proc. Tech.* **35**, 55 (1993).
3. Weisz, P. B., *Adv. Catal.* **13**, 137 (1962).
4. Coonradt, H. L., and Garwood, W. E., *Ind. Eng. Chem. Res. Process Des. Dev.* **3**, 38 (1964).
5. Steijns, M., and Froment, G. F., *Ind. Eng. Chem. Res. Prod. Res. Dev.* **20**, 660 (1981).
6. Weitkamp, J., *Erdol Kohle Erdgas P.* **31**, 13 (1978).
7. Kazansky, V. B., Frash, M. V., and van Santen, R. A., *Appl. Catal. A: Gen.* **146**, 225 (1996).
8. Rigby, A. M., Kramer, G. J., and van Santen, R. A., *J. Catal.* **170**, 1 (1997), doi:10.1006/jcat.1997.1574.
9. Natal-Santiago, M. A., Alcala, R., and Dumesic, J. A., *J. Catal.* **181**, 124 (1999), doi:10.1006/jcat.1998.2293.
10. Martens, J. A., and Jacobs, P. A., *in* "Handbook of Heterogeneous Catalysis" (G. Ertl, H. Knözinger, and J. Weitkamp, Eds.), p. 1137. VCH, Weinheim/New York, 1997.
11. Svoboda, G. D., Vynckier, E., Debrabandere, B., and Froment, G. F., *Ind. Eng. Chem. Res.* **34**, 3793 (1995).
12. Martens, G. G., Marin, G. B., Martens, J. A., Jacobs, P. A., and Baron, G. V., *J. Catal.* **195**, 253 (2000), doi:10.1006/jcat.2000.2993.
13. Kerr, G. T., *Adv. Chem. Ser.* **121**, 219 (1972).
14. Wang, Q. L., Giannetto, G., Torrealba, M., Perot, G., Kappenstein, C., and Guisnet, M., *J. Catal.* **130**, 459 (1991).
15. Barthomeuf, D., *Mat. Chem. Phys.* **17**, 49 (1987).
16. Kuehne, M. A., Kung, H. H., and Miller, J. T., *J. Catal.* **171**, 293 (1997), doi:10.1006/jcat.1997.1825.
17. Corma, A., Martinez, A., Pergher, S., Peratello, S., Perego, C., and Bellusi, G., *Appl. Catal. A: Gen.* **152**, 107 (1997).
18. Kuehne, M. A., Babitz, S. M., Kung, H. H., and Miller, J. T., *Appl. Catal. A: Gen.* **166**, 293 (1998).
19. Morin, S., Ayrault, P., Gnep, N. S., and Guisnet, M., *Appl. Catal. A: Gen.* **166**, 281 (1998).
20. Zhang, W., and Smirniotis, P. G., *J. Catal.* **182**, 400 (1999), doi:10.1006/jcat.1998.2337.
21. Yaluris, G., Madon, R. J., and Dumesic, J. A., *J. Catal.* **186**, 134 (1999), doi:10.1006/jcat.1999.2537.
22. Dempsey, E., *J. Catal.* **33**, 497 (1974).
23. van Santen, R. A., and Kramer, G. J., *Chem. Rev.* **95**, 637 (1995).
24. Remy, M. J., Stanica, D., Poncelet, G., Feijen, E. J. P., Grobet, P. J., Martens, J. A., and Jacobs, P. A., *J. Phys. Chem.* **100**, 12,440 (1996).
25. Wouters, B. H., Chen, T.-H., and Grobet, P. J., *J. Am. Chem. Soc.* **120**, 11419 (1998).
26. Wang, Q. L., Giannetto, G., and Guisnet, M., *J. Catal.* **130**, 471 (1991).
27. Biaglow, A. I., Parillo, D. J., Kokotailo, G. T., and Gorte, R. J., *J. Catal.* **148**, 213 (1994), doi:10.1006/jcat.1994.1203.
28. Bamwenda, G. R., Zhao, Y. X., Groten, W. A., and Wojciechowski B. W., *J. Catal.* **157**, 209 (1995), doi:10.1006/jcat.1995.1281.
29. Debrabandere, D., and Froment, G. F., *Stud. Surf. Sci. Catal.* **106**, 379 (1997).
30. Denayer, J. F., Baron, G. V., Souverijns, W., Martens, J. A., and Jacobs, P. A., *Ind. Eng. Chem. Res.* **36**, 3242 (1997).
31. Collignon, F., Mariani, M., Moreno, S., Remy, M., and Poncelet, G., *J. Catal.* **166**, 53 (1997), doi:10.1006/jcat.1997.1503.
32. Niwa, M., Katada, N., Sawa, M., and Murakami, Y., *J. Phys. Chem.* **99**, 8812 (1995).
33. Denayer, J. F. M., and Baron, G. V., *Adsorption* **3**, 1 (1997).
34. Denayer, J. F., Baron, G. V., Vanbutsele, G., Jacobs, P. A., and Martens, J. A., *J. Catal.* **190**, 469 (2000), doi:10.1006/jcat.1999.2756.
35. Rosenbrock, H. H., *Comput. J.* **3**, 175 (1960).
36. Marquardt, D. W., *Ind. Appl. Math.* **11**, 431 (1963).
37. Netlib, http://www.netlib.org.
38. Boggs, P. T., Byrd, R. H., Rogers, J. E., and Schnabel, R. B., *NISTIR* **92**-4834 (1992).
39. Froment, G. F., and Bischoff, K. B., "Chemical Reactor Analysis and Design," 2nd ed. Wiley, New York, 1990.
40. Byrne, G. D., and Hindmarsch, A. C., *J. Comp. Phys.* **70**, 1 (1987).

41. Petzold, L. R., *Siam. J. Sci. Stat. Comput.* **4**, 136 (1983).
42. Vynckier, E., and Froment, G. F., *in* "Kinetic and Thermodynamic Lumping of Multicomponent Mixtures" (G. Astarita and S. I. Sandler, Eds.). Elsevier, Amsterdam, 1991.
43. Benson, S. W., Cruickshank, F. R., Golden, D. M., Haugen, G. R., O'Neal, H. E., Rodgers, A. S., Shaw, R., and Walsch, R., *Chem. Rev.* **69**, 279 (1969).
44. Denayer, J. F., Baron, G. V., Martens, J. A., and Jacobs, P. A., *J. Phys. Chem. B* **102**, 3077 (1998).
45. Denayer, J. F., Baron, G. V., Jacobs, P. A., and Martens, J. A., *Phys. Chem. Chem. Phys.* **2**, 1007 (2000).
46. Vansina, H, Baltanas, M. A., and Froment, G. F., *Ind. Eng. Chem. Prod. Res. Dev.* **22**, 526 (1983).
47. Corma, A., Lopez Aguado, A., Nebot, I., and Tomas, F., *J. Catal.* **77**, 159 (1982).
48. Martens, J. A., and Jacobs, P. A., *in* "Theoretical Aspects of Heterogeneous Catalysis" (J. B. Moffat, Ed.), Van Nostrand Reinhold catalysis series, 1990.
49. Yaluris, G., Madon, R. J., Rudd, D. F., and Dumesic, J. A., *Ind. Eng. Chem. Res.* **33**, 2913 (1994).
50. Yaluris, G., Rekoske, J. E., Aparicio, L. M., Madon, R. J., and Dumesic, J. A., *J. Catal.* **153**, 54 (1995), doi:10.1006/jcat.1995.1107.
51. Watson, B. A., Klein, M. T., and Harding, R. H., *Ind. Eng. Chem. Res.* **35**, 1506 (1996).
52. Watson, B. A., Klein, M. T., and Harding, R. H., *Appl. Catal. A: Gen.* **160**, 13 (1997).
53. Watson, B. A., Klein, M. T., and Harding, R. H., *Ind. Eng. Chem. Res.* **36**, 2954 (1997).
54. Dumesic, J. A., Rudd, D. F., Aparicio, L. M., Rekoske, J. E., and Treviño, A. A., "The Microkinetics of Heterogeneous Catalysis." Am. Chem. Soc., Washington, DC, 1993.
55. Boudart, M., and Djéga-Mariadassou, G., "Kinetics of Heterogeneous Catalytic Reactions." Princeton Univ. Press, Princeton, NJ, 1984.
56. Beirnaert, H. C., Alleman, J. R., and Marin, G. B., *Ind. Eng. Chem. Res.* **40**, 1337 (2001).